3D Motion Planning for Robot-Assisted Active Flexible Needle Based on Rapidly-Exploring Random Trees

Yan-Jiang Zhao
Department of Radiation Oncology, Thomas Jefferson University, Philadelphia, PA19107, USA
Intelligent Machine Institute, Harbin University of Science and Technology, Harbin 150080, China
Email: Yanjiang.Zhao@jefferson.edu; zhaoyj@hrbust.edu.cn

Bardia Konh and Mohammad Honarvar
Department of Mechanical Engineering, Temple University, Philadelphia, PA 19122 USA
Email: {konh, Mohammad.Honarvar}@temple.edu

Felix Orlando Maria Joseph and Tarun K. Podder
Department of Radiation Oncology, Case Western Reserve University, Cleveland, OH 44106 USA
Email: {fom, tarun.podder}@case.edu

Parsaoran Hutapea
Department of Mechanical Engineering, Temple University, Philadelphia, PA 19122 USA
Email: hutapea@temple.edu

Adam P. Dicker and Yan Yu
Department of Radiation Oncology, Thomas Jefferson University, Philadelphia, PA 19107 USA
Email: {Adam.Dicker, Yan.Yu}@jefferson.edu

***Abstract*—An active flexible needle is a self-actuating needle that can bend in the tissue and reach the clinical targets while avoiding anatomic obstacles. In robot-assisted needle-based medical procedures, motion planning is a vital aspect of operations. It is challenging due to the nonholonomic motion of the needle and the presence of anatomic obstacles and sensitive organs that must be avoided. We propose a novel and fast motion planning algorithm for the robot-assisted active flexible needle. The algorithm is based on Rapidly-Exploring Random Trees combined with greedy-heuristic strategy and reachability-guided strategy. Linear segment and relaxation of insertion orientation are taken into consideration to the paths. Results show that the proposed algorithm yields superior results as compared to the commonly used algorithm in terms of computational speed, form of path and robustness of searching ability, which potentially make it suitable for the real-time intraoperative planning in clinical operations.**

***Index Terms*—active flexible needle, motion planning, rapidly-exploring random tree, nonholonomic system, minimally invasive surgery, robot assisted surgery**

I. Introduction

Needle insertion is probably one of the most pervasive procedures in minimally invasive surgeries, such as tissue biopsies and radioactive seed implantations for cancers. However, the target may be located in a region surrounded by anatomic obstacles or sensitive organs that must be avoided. Traditional rigid needles can hardly meet these needs. As an alternative to the traditional rigid needles, we have been developing a flexible needle which is an active or self-actuating (symmetric-tip) flexible needle other than passive (bevel-tip) flexible needles, see Fig. 1 [1]. Utilizing the characteristic of shape memory alloys (SMA), the needle can generate a variety of curvatures of paths by supplying different electric currents to the SMA actuators [2]-[5].

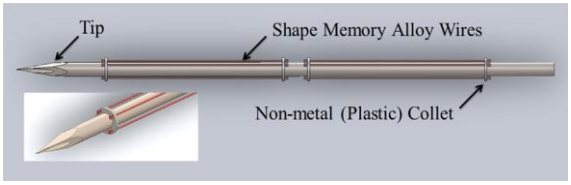

Figure 1. Schematic of an active flexible surgical needle

In robot-assisted needle insertion procedures, motion planning is a critical aspect for navigating a robot and a needle to gain an accurate and safe operation. However, steering a flexible needle in the soft tissue is challenging due to the nonholonomic motion of the needle and the presence of anatomic obstacles and sensitive organs. In recent years, motion planning for flexible needles has

Manuscript received August 14, 2014; revised December 2, 2014.

doi: 10.12720/joace.3.5.360-367

been extensively studied in different approaches in 2D and 3D environments with obstacles [6]-[18].

One popular approach is mathematical computation method, which formulates the problem as an optimization problem with an objective function and computes the optimal solution. Duindam *et al.* presented a screw-based motion planning algorithm using an optimizing function [6], and he also proposed an inverse kinematics motion planning algorithm based on mathematical calculation [7]. Park *et al.* proposed a path-of-probability algorithm to optimize the paths by computing the probability density function [8]. Alterovitz *et al.* formulated the path planning problem of bevel tip flexible needles as a Markov Decision Process to maximize the probability of successfully reaching the target in a 2D environment [9]. The mathematical computation method usually has a computational expense and may suffer from stability/convergence. Therefore, they are often used for preoperative planning, but not appropriate for intraoperative planning.

Another important approach is sampling-based method, such as the Probabilistic Roadmaps (PRM) or the Rapidly-Exploring Random Tree (RRT). Alterovitz et al. proposed a path planner for Markov uncertain motion base on PRM [10]. Lobaton *et al.* presented a PRM-based method for planning paths that visit multiple goals [11]. Since Xu *et al.* firstly applied RRT-based method to search a valid needle path in a 3D environment with obstacles [12], the RRT algorithm is commonly used in flexible needle path planning. Patil *et al.* greatly sped up the calculation utilizing a modified version of RRT method that combines the reachability guided and goal bias strategies (RGGB-RRTs) [13], which was then extended into a dynamic environment replanning [14]. The RGGB-RRTs is the most commonly used algorithm nowadays. Caborni *et al.* proposed a risk-based path planning for a steerable flexible probe based on the RGGB-RRTs [15]. Recently, Vrooijink *et al.* proposed a rapid replanning algorithm based on the RGGB-RRTs, and embedded it into a control system [16]. Bernardes et al. presented a fast intraoperative replanning algorithm based on the RGGB-RRTs in 2D and 3D environments [17]-[18].

In summary, firstly, all the algorithms are only aiming at utilizing the curvilinear paths, but not considering the linear segments, which may both shorten the length of path and save the cost of control and energy for the active needle (because you do not have to make the needle bent by actuators). Although Patil et al. relaxed the curvatures of the curvilinear paths which allowed the linear segments in the paths theoretically, because of the probabilistic nature of the RRT algorithm, the possibility for the appearance of the linear segment is nearly non-existent [13]. Secondly, most of the algorithms, if not all, are with the routine method that the insertion orientation is fixed or specified, e.g. to be orthogonal to the skin surface, therefore the planning or optimizing results are constrained originally. Although Xu *et al.* relaxed the insertion orientation by a back-chaining method, the orientation of approaching to the goal is fixed originally [12].

In this paper, a novel and fast motion planning algorithm based on RRT is proposed for the active flexible needle. We propose a greedy heuristic strategy using the Depth First Search (DFS) method, and combine it with the reachablility-guided strategy to improve the conventional RRT [19]. It is named as Greedy Heuristic and Reachability-Guided Rapidly-Exploring Random Trees (GHRG-RRTs). We adopt variable but bounded curvatures of the needle paths, and we also take account of linear segments and relaxation of insertion orientations to the trajectories.

II. Kinematic Model of Active Flexible Needle

Different with the bevel tip needles (with two DOFs: insertion and rotation) [20], the active flexible needle has three DOFs: insertion, rotation and tip bending (relative to u_1, u_2 and electrical current I, respectively. See Fig. 2). There is a connection joint between the needle body and needle tip. The different radii of paths are attained by means of the different bending of the tip. And the kinematic model of the active flexible needle is formulated as follows (see Fig. 2). The position and orientation of the connection joint relative to frame Ψ_w can be described compactly by a 4×4 homogeneous transformation matrix

$$\boldsymbol{g}_{wn} = \begin{bmatrix} \boldsymbol{R}_{wn} & \boldsymbol{p}_{wn} \\ 0 & 1 \end{bmatrix} \in \boldsymbol{SE}(3) \tag{1}$$

where $\boldsymbol{R}_{wn} \in \boldsymbol{SO}(3)$ and $\boldsymbol{p}_{wn} \in \boldsymbol{R}^3$ are the rotation matrix and the position of frame Ψ_n relative to frame Ψ_w, respectively.

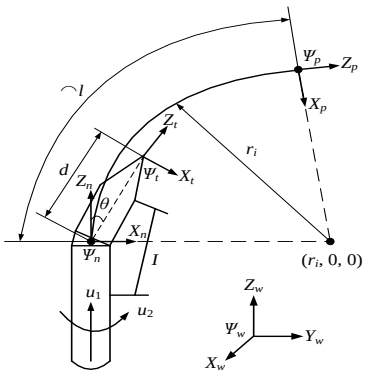

Figure 2. Kinematic model of the active flexible needle

If we use the connection joint part as the end-effector of the needle, while the needle tip working as a navigator, we can disregard the position of the needle tip by expanding the obstacles with a safty belt d.

Then, the homogeneous transformation matrix can be formulated in the exponential form

$$\boldsymbol{g}_{wn}(T) = \boldsymbol{g}_{wn}(0) \prod_{i=1}^{N} \exp(\hat{\boldsymbol{\xi}}_i t_i) \tag{2}$$

where $\boldsymbol{g}_{wn}(0)$ is the initial configuration of the needle (frame Ψ_n) in frame Ψ_w before insertion; t_i is the performance time of the i^{th} segment; T is the total time of

the performance of the whole path, $T = \sum_{i=1}^{n} t_i$. Details could be attained in [20].

We coincide frame Ψ_n and frame Ψ_w initially, and consider the insertion pose (rotating β_0 around axis Y_w and then rotating α_0 around axis Z_w), hence, the configurations of the insertion pose can be obtained by

$$\boldsymbol{g}_{wn}(0) = Rot(Z_w, \alpha_0) Rot(Y_w, \beta_0) \quad (3)$$

Since the inputs drive the needle to perform a geometric trajectory, we can encode the trajectory with geometric parameters instead of the actual control inputs $\boldsymbol{U}$: (u_1, u_2, I), in order to avoid the inefficient performance that randomly samples control inputs to compute the best combination [12]. The path is composed of a series of segments $\{C_1, C_2, \ldots, C_N\}$ [13], each of which C_i can be parameterized as $\boldsymbol{U}_i$: (α_i, r_i, l_i), where α_i is the rotation angle of the needle shaft (corresponding to u_2), r_i is the radius of the i^{th} arc (which is infinite if a linear segment, corresponding to I), and l_i is the length of the i^{th} segment (corresponding to u_1). The transformation matrix for each segment $\boldsymbol{g}_i$ can be formulated by $\boldsymbol{U}_i$ (details are available in Sec. III D).

III. Motion Planning Algorithm

The needle motion planning problem is to determine an optimal geometric trajectory using an efficient planner, from which the control plans will be generated so that the needle tip reaches the specified target while avoiding anatomic obstacles. The algorithm can be divided into two parts: one is to generate candidate solutions of paths using a sample-based method, and the other is to find the optimal path based on an objective function. The paths must be complied with the kinematic constraints of the needle. They are smooth and with relaxed but bounded curvatures, including linear segments.

A. Outline of GHRG-RRTs Algorithm

The program is as shown in Algorithm 1. Unlike other RRT algorithms, once initialized with q_{init}, this algorithm does not immediately generate a random node, instead, it verifies whether a path can be generated directly from q_{init} to q_{goal} including linear or curvilinear collision-free path (lines 2-10). If a linear path is achieved, the searching finishes because obviously, it is the best path. If not, it verifies a curvilinear path. And then the algorithm goes into the loop programs. The algorithm begins to generate a random node q_{rand} by the routine RandomNode(). And then it searches for trees and paths in a greedy heuristic way and iterates until the terminate condition is reached.

Algorithm 1: GHRG-RRTs (q_{init}, q_{goal}, $\boldsymbol{Q}$)

1: $\boldsymbol{T} \leftarrow$ InitTree(q_{init}); $\boldsymbol{P} \leftarrow$ InitPath(q_{init});
2: **if** LinearCheck(q_{init}, q_{goal}, $\boldsymbol{Q}$)
3: $\boldsymbol{U} \leftarrow$ SolveLine(q_{init}, q_{goal})
4: $\boldsymbol{P} \leftarrow$ AchivePath($\boldsymbol{T}$, $\boldsymbol{U}$, q_{goal})
5: **return** $\boldsymbol{P}$ } Get a linear path
6: **end if**
7: $\boldsymbol{U} \leftarrow$ SolveSeg($\boldsymbol{T}.\boldsymbol{g}_{init}$, q_{goal})
8: **if** $\boldsymbol{U}.r \geq r_{min}$ **&** CollisionFree($\boldsymbol{U}$, $\boldsymbol{Q}$)
9: $\boldsymbol{P} \leftarrow$ AchivePath($\boldsymbol{T}$, $\boldsymbol{U}$, q_{goal}) } Get a curve path
10: **end if**
11: **while** ($n < max\_path$) & ($i < max\_iteration$)
12: $q_{rand} \leftarrow$ RandomNode(); flag $\leftarrow$ false
13: **if** LinearCheck(q_{init}, q_{rand})
14: $\boldsymbol{U} \leftarrow$ SolveLine(q_{init}, q_{rand}) } Get a linear tree
15: $\boldsymbol{T} \leftarrow$ ExtendTree ($\boldsymbol{T}$, $\boldsymbol{U}$, q_{rand})
16: $\boldsymbol{U} \leftarrow$ SolveSeg($\boldsymbol{T}.\boldsymbol{g}_{rand}$, q_{goal})
17: **if** $\boldsymbol{U}.r \geq r_{min}$ **&** CollisionFree($\boldsymbol{U}$, $\boldsymbol{Q}$)
18: $\boldsymbol{P} \leftarrow$ AchievePath ($\boldsymbol{T}$, $\boldsymbol{U}$, q_{goal}); flag $\leftarrow$ true } Get a path
19: **end if**
20: **end if**
21: $\boldsymbol{U} \leftarrow$ SolveSeg(q_{init}, q_{rand})
22: **if** $\boldsymbol{U}.r \geq r_{min}$ **&** CollisionFree($\boldsymbol{U}$, $\boldsymbol{Q}$)
23: $\boldsymbol{T} \leftarrow$ ExtendTree ($\boldsymbol{T}$, $\boldsymbol{U}$, q_{rand}) } Get a curve tree
24: **end if**
25: $\boldsymbol{U} \leftarrow$ SolveSeg($\boldsymbol{T}.\boldsymbol{g}_{rand}$, q_{goal})
26: **if** $\boldsymbol{U}.r \geq r_{min}$ **&** CollisionFree($\boldsymbol{U}$, $\boldsymbol{Q}$)
27: $\boldsymbol{P} \leftarrow$ AchievePath ($\boldsymbol{T}$, $\boldsymbol{U}$, q_{goal}); flag $\leftarrow$ true } Get a path
28: **end if**
29: **if** flag==false
30: $q_{proper} \leftarrow$ FindProperNode ($\boldsymbol{T}$, q_{rand}, ρ)
31: $\boldsymbol{U} \leftarrow$SolveSeg($\boldsymbol{T}.\boldsymbol{g}_{proper}$, q_{rand})
32: **if** $\boldsymbol{U}.r \geq r_{min}$ **&** CollisionFree($\boldsymbol{U}$, $\boldsymbol{Q}$)
33: $\boldsymbol{T} \leftarrow$ ExtendTree ($\boldsymbol{T}$, $\boldsymbol{U}$, q_{rand}) } Extend a tree
34: $\boldsymbol{U} \leftarrow$ SolveSeg($\boldsymbol{T}.\boldsymbol{g}_{rand}$, q_{goal})
35: **if** $\boldsymbol{U}.r \geq r_{min}$ **&** CollisionFree($\boldsymbol{U}$, $\boldsymbol{Q}$)
36: $\boldsymbol{P} \leftarrow$ AchievePath ($\boldsymbol{T}$, $\boldsymbol{U}$, q_{goal}) } Get a path
37: **end if**
38: **end if**
39: **end while**
40: $p_{opt} \leftarrow$ Optimization($\boldsymbol{P}$)
41: **return** p_{opt}

AchievePath ($\boldsymbol{T}$, $\boldsymbol{U}$, q_{goal})
1: $\boldsymbol{T} \leftarrow$ExtendTree ($\boldsymbol{T}$, $\boldsymbol{U}$, q_{goal})
2: $p \leftarrow$ ExtractPath($\boldsymbol{T}$)
3: $\boldsymbol{P}$.add_path(p)
4: **return** $\boldsymbol{P}$

ExtendTree ($\boldsymbol{T}$, $\boldsymbol{U}$, q)
1: $\boldsymbol{g} \leftarrow$ GetConfig($\boldsymbol{U}$, q)
2: $\boldsymbol{T}$. add_vertex(q)
3: $\boldsymbol{T}$. add_edge(q, $\boldsymbol{g}$)
4: **return** $\boldsymbol{T}$

B. Greedy-Heuristic Strategy

In contrast to all the previous RRT algorithms, we propose a greedy heuristic strategy to generate more trees and complete more paths: on the one hand, it is greedy for initial node to generate a new tree; on the other hand, it is greedy for the goal node to achieve a path. After a valid random node is obtained, the algorithm will verify whether a linear segment could be generated connecting the initial node q_{init} to the random node q_{rand}, if yes, a new tree starting with a linear segment will be generated (lines 13-15). By doing so, it successfully relaxes the insertion orientations, which can be in various angles rather than just orthogonal to the skin surface. If the tree is generated, it goes on to verify whether q_{rand} can connect q_{goal} (lines 16-19), if yes, a new path will be gained. Here we are greedy for searching the goal, because we believe that the direct connection from q_{rand} to q_{goal} is probabilistically superior to those which travel round and then connect to the goal. This strategy is also with an idea of DFS to effectively achieve goals. Then it will search for a curvilinear path with the similar process (lines 21-28). If no path is gained after above searching, it will try to extend the other trees that have not been achieved a path (line 29-33). In contrast to searching for a nearest node in the previous algorithms, it searches for a proper node q_{proper} (by routine 30). The proper node should be amid all the nodes but for the initial node q_{init} and the goal node q_{goal} in all trees that have not been achieved a path. The

idea of the proper node means the node should not be too near to an existing node, the distance should be larger than a specific metric ρ in order to prevent the insufficient growth. It is the nearest node in those whose distances to q_{rand} are larger than ρ. After q_{proper} is acquired, from which the algorithm will extend the tree to q_{rand}, then try to achieve a path by similar means (lines 21-28).

C. Reachability-Guided Strategy

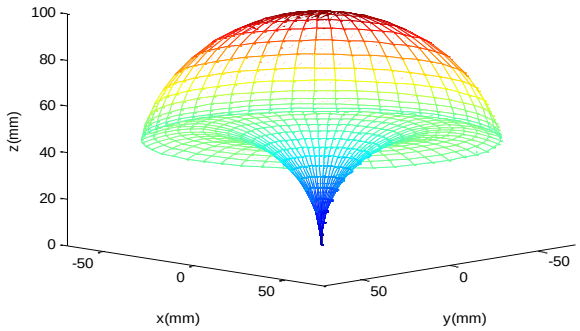

(a) Reachable region in 3D

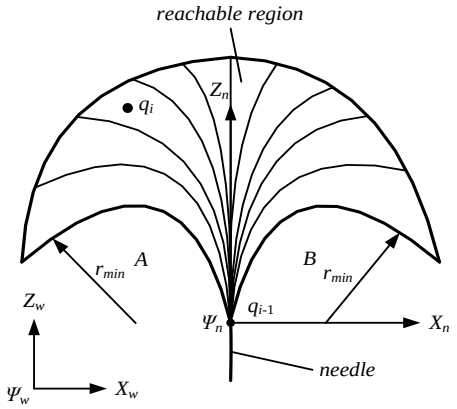

(b) Reachable region in 2D

Figure 3. Reachable Region of the Needle

The path is composed of a series of segments, each of which the final extremity corresponds to the next segment's initial extremity, not only in position but also in orientation, because of the presence of the nonholonomic constraints. Hence, it is possible that a node is not reachable for a specific extremity (with a specific configuration). The reachable region of the needle is a mushroom-like area as shown in Fig. 3(a). In order to elaborate the problem, we project it into 2D (*XOZ* plane), which is a leaf-like area as shown in Fig. 3(b). From q_{i-1} in a local frame Ψ_n, the reachable region will extend with the depth of insertion, but no matter how deeply it is inserted, there always are two regions of ***A*** and ***B*** that cannot be reached. There is a minimum bending radius r_{min} for the needle path corresponding to the mechanical properties of the needle. In order to speed up the search and make the following calculation effective, the reachability of the next node q_i (may be q_{goal} or q_{rand}) should be checked. According to the Fig. 3, the next node is reachable as long as

$$r_i \geq r_{min} \tag{4}$$

where r_i is the radius of the i^{th} segment (from q_{i-1} to q_i), one of the input parameters, and can be obtained in the next section; r_{min} is the minimum radius constraint of the needle path.

Different from the reachability-guided strategy proposed in [13], we directly use one of the input parameters as a judgment, instead of bringing in extra calculations, which is beneficial for speeding up the search [18].

D. Input Parameter U and Configuratiog

Because we have considered the insertion pose, there are two additional parameters before insertion: α_0 and β_0 as mentioned in Sec. 2. For a path starting with a curvilinear segment, they are generated randomly by the planner; for a linear path or a path starting with a linear segment, they are obtained by (5-6). And then the insertion pose $\boldsymbol{g}_{wn}(0)$ is calculated by (4).

$$\alpha_0 = \begin{cases} \arctan(y_n / x_n), & x \geq 0 \\ \pi + \arctan(y_n / x_n), & x < 0 \end{cases} \tag{5}$$

$$\beta_0 = \arctan(k / z_n) \tag{6}$$

where x_n, y_n, z_n are the coordinates of the next node q_i in frame Ψ_n, which is initially coincided with frame Ψ_w; $k = \sqrt{x_n^2 + y_n^2}$.

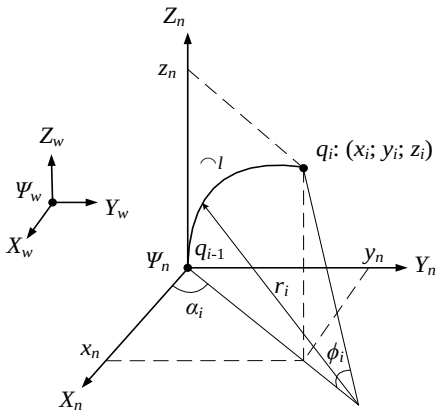

Figure 4. Input of the i^{th} segment

Assume that the extremity q_i of the i^{th} segment is with an input $\boldsymbol{U}_i$ operating from q_{i-1}, and is with a subsequent transformation matrix $\boldsymbol{g}_i$ in the form as (1). A local frame Ψ_n is attached to q_{i-1} as is shown in Fig. 4. The coordinates of q_i: (x_i; y_i; z_i) in frame Ψ_w are converted into frame Ψ_n as q_i: (x_n; y_n; z_n), ϕ_i is the angle embraced by the circular arc. So the input $\boldsymbol{U}_i$: (α_i, r_i, l_i) can be formulated as follows:

$$r_i = k/2 + z_n^2 / 2k \tag{7}$$

$$\phi_i = \pi - 2\arctan(z_n / k) \tag{8}$$

$$l_i = r_i \times \phi_i \tag{9}$$

The input α_i can be calculated by (5), and the transformation matrix $\boldsymbol{g}_i$ obtained by

$$\boldsymbol{g}_i = \begin{bmatrix} \cos\alpha_i \cos\phi_i & -\sin\alpha_i & \cos\alpha_i \sin\phi_i & x_n \\ \sin\alpha_i \cos\phi_i & \cos\alpha_i & \sin\alpha_i \sin\phi_i & y_n \\ -\sin\phi_i & 0 & \cos\phi_i & z_n \\ 0 & 0 & 0 & 1 \end{bmatrix} \quad (10)$$

The configuration of the end-effector $\boldsymbol{g}_{wn}$ can be obtained by (2).

E. Optimization Function

Among the candidate solutions, all of which have already met the required constraints, the optimal path can be chosen based on a cost function. The objectives of the optimization will take consideration of minimizing the tissue trauma, enhancing the accuracy, and minimizing the force-torque on the needle as well as the temperature rise.

$$\min F(\boldsymbol{u}, T) = \min\{\alpha_1 L + \alpha_2 D + \alpha_3 S + \alpha_4 N\} \quad (11)$$

where L is the length of the path; D is the degree of danger in the path, relative to the distance between the path and the obstacles; S is the curve valuation of the path, evaluated by curvatures, which is relative to the force-torque on the needle as well as the temperature rise; N is the degree of control, i.e. the number of segments of the whole path, which is relative to the control cost and accuracy [21]; α_1~α_4 are the weighted coefficients. The result of the function is the comprehensive evaluation of the optimal path.

IV. Simulation Results and Discussion

We simulated the motion planner in MATLAB® (ver. 7.8.0, R2009a; MathWorks, Natick, MA) on a 2.5 GHz 4-core Intel® i5™ PC. We firslty set the minmum radius $r_{\min}$=50mm [13], [22], the specific metric ρ=10mm. The maximum number of the candidate paths is set to 100, and the maximum number of iterations to 10000. Assuming that the obstacle is containing a relative belt of safe margin around it, in order to speed up the computation, we can disregard the second term in (11) by setting α_2=0. The weighted coefficients α_1=α_3=α_4=1. In order to compare the performances of the GHRG-RRTs algorithm and the RGGB-RRTs algorithm, we set the goal bias factor to 0.2 as in [15].

A. Test Case 1

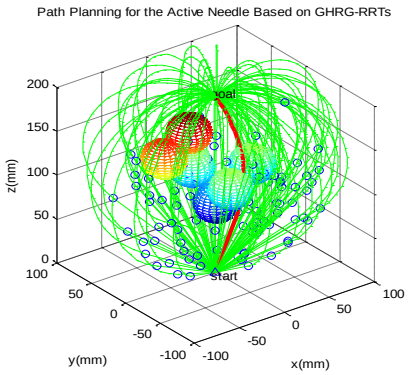

(a) GHRG-RRTs algorithm

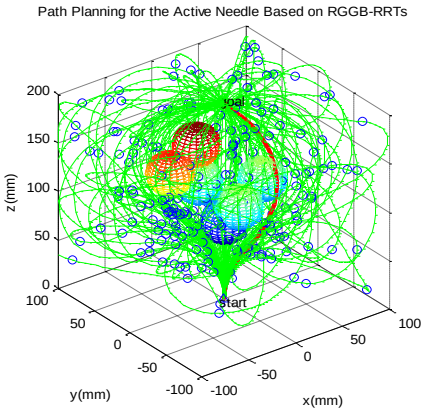

(b) RGGB-RRTs algorithm

Figure 5. Results of one simulation for the two approaches

We define the envorinment similar to [12], [13], modeling as a cubical region with 200mm along each axis. Six spherical obstacles, each of radii 20mm, representing the pubic arch, the urethra, and the penile bulb around the prostate.

Fig. 5 shows the results of one simulation for the two approaches, respectively. We have also performed 50 trials and achieved all the optimal results of the two approaches as dipicted in Fig. 6 as well as in Table I. In the figures, the spheres are the obstacles, the small blue circles are the conjunction points of the two segments in the paths, the green lines are the feasible paths, and the red lines are the optimal ones. In the tables, the results are with the formation of "mean ± standard deviation" of the 50 trials.

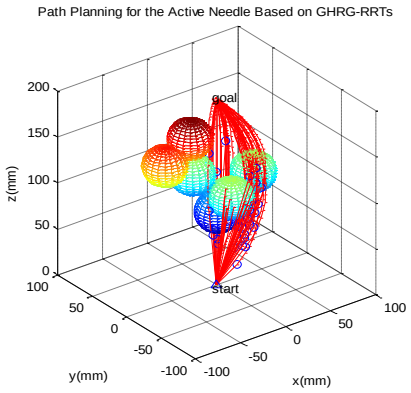

(a) GHRG-RRTs algorithm

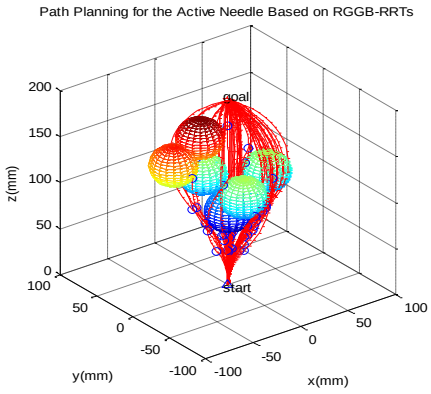

(b) RGGB-RRTs algorithm

Figure 6. Optimal results of the 50 trials

TABLE I. COMPARISON BETWEEN THE TWO APPROACHES

Approach	CPU time for one tree (ms)	Value of function	Length of path	No. of iterations
GHRG-RRTs	1.3±0.0001	218.10±6.21	215.54±6.14	285±22
RGGB-RRTs	122.7±166.9	223.40±7.30	220.26±7.18	2476±335

From the results of the above both cases, we can conclude that: (1) the GHRG-RRTs algorithm can effeciently achieve variety of the paths with linear segments as well as curved segments, and the optimal path is likely to be the one with linear segments; (2) the GHRG-RRTs algorithm is superior to the RGGB-RRTs algorithm thoroughly: the speed is nearly 100 times faster, the optimial path is always better, and the number of iterations is much smaller.

B. *Test Case 2*

In order to test and compare the two algorithms further, we have created a more complex environment by compressing the environments and adding extra obstacles. We have shrunk the environments into half and then added an additional obstacle to the envrionment (see Fig. 7). We added an obstacle lacated at (0; 0; 25), with radius 10mm. The maxmum iteration number is set to 50000, other settings are the same as the former.

While the RGGB-RRTs algorithm failes to obtain any solution, the RGHG-RRTs algorithm successfully and rapidly achieves 100 trajectories and the optimal one is calculated. We have also performed 50 trials of the opimizations, results are as shown in Fig. 7 and Table II.

It is of great significance to poit it out that the reason for the RGGB-RRTs planner can not find any solution is not because of the maximum iteration number is not large enough, but it is because there is no solution indeed, with the specific configuration (orthogonal to the surface) in the environment, which can be proved in a geometric calculation. In the contrast, GHRG-RRTs algorithm relaxes the insertion orientations and gains a solution in a fast speed.

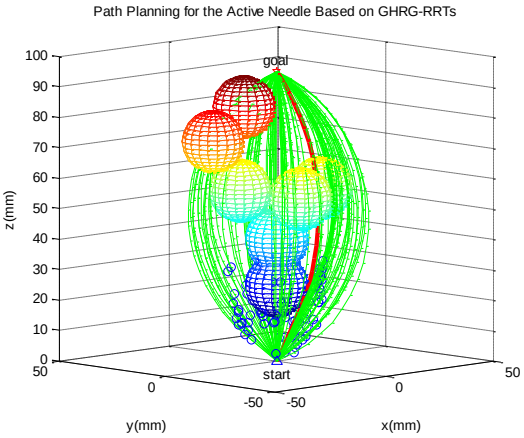

(a) result of one simulation

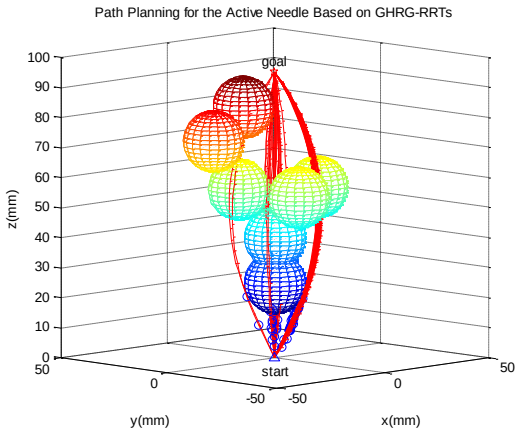

(b) results of 50 trials

Figure 7. Results of RGHG-RRTs

TABLE II. PERFORMANCES OF GHRG-RRTS

Approach	CPU time for one tree (ms)	Value of function	Length of path	No. of iterations
GHRG-RRTs	53.1±4.4	103.38±0.54	100.76±0.51	18730±1521

Results show that the GHRG-RRTs algorithm has a robust searching ability. It enhances the possibility for an optimal solution by relaxing the insertion orientation. Although the searching efficiency has suffered from the complexity of environment compared to the former cases, it is still very fast.

V. CONCLUSION

We proposed a novel and fast path planning algorithm named GHRG-RRTs algorithm which is developed based on RRT for a robot-assisted active flexible needle steering. We formulated a greedy-heuristic strategy and combined it with the reachability-guided strategy to speed up the search and to improve the convergence. We adopted the linear segments to the paths, and the insertion directions are relaxed by the introduction of the linear segments. We also formulated an optimizing function, by which the optimal path can be achieved from the sub-optimal candidate paths. Simulation tests were done in 3D environments with obstacles. In comparison with the RGGB-RRTs algorithm, the performance of the proposed GHRG-RRTs algorithm was superior in terms of computational speed, form of path and robustness of searching ability. This high efficiency and robustness make it a possibility for intraoperative motion planning in clinical procedures.

In the future work, we will extend this algorithm into a 3D dynamic environment to achieve the real-time intraoperative planning for clinical operations, considering the uncertainties or errors due to tissue heterogeneity, tissue deformation, needle modeling as well as tip tracking. And then we will integrate our planner with a real-time feedback controller and carry out experiments on tissue phantoms and animal ex vivo tissues.

ACKNOWLEDGMENT

This research is supported in part by the Department of Defense CDMRP Prostate Cancer Research Program (Grants# W81XWH-11-1-0397/98/99), by National Natural Science Foundation of China (Grant# 51305107) and by Science and Technology Project of Heilongjiang Provincial Education Department, China (Grant# 12531110).

REFERENCES

[1] T. K. Podder, A. P. Dicker, P. Hutapea, K. Darvish, and Y. Yu, "A novel curvilinear approach for prostate seed implantation," *Med. Phys.*, vol. 39, no. 4, pp. 1887-1892, Apr. 2012.
[2] N. V. Datla, M. Honarvar, T. M. Nguyen, B. Konh, K. Darvish, Y. Yu, *et al*., "Toward a nitinol actuator for an active surgical needle," in *Proc. ASME Conference on Smart Material, Adaptive Structures and Intelligent Systems*, 2012, pp. 19-21.
[3] B. Konh, N. V. Datla, M. Honarvar, T. K. Podder, A. P. Dicker, Y. Yu, and P. Hutapea, "Design exploration study of a shape memory alloy actuated surgical needle," *Journal of Intelligent Material Systems and Structures*, in press.
[4] M. Honarvar, N. V. Datla, B. Konh, T. K. Podder, A. P. Dicker, Y. Yu, and P. Hutapea, "Study of unrecovered strain and critical stresses in one-way shape memory nitinol," *Journal of Materials Engineering and Performance*, in press.
[5] B. Konh, M. Honarvar, and P. Hutapea, "Application of SMA wire for an active steerable cannula," in *Proc. ASME Conference on Smart Materials, Adaptive Structures and Intelligent Systems*, 2013, pp. 265-269.
[6] V. Duindam, R. Alterovitz, S. Sastry, and K. Goldberg, "Screw-based motion planning for bevel-tip flexible needles in 3D environments with obstacles," in *Proc. IEEE Int. Conf. on Robotics and Automation*, 2008, pp. 2483-2488.
[7] V. Duindam, J. Xu, R. Alterovitz, S. Sastry, and K. Goldberg, "Three-dimensional motion planning algorithms for steerable needles using inverse kinematics," *Int. Journal of Robotics Research*, vol. 29, no. 7, pp. 789-800, June 2010.
[8] W. Park, Y. Wang, and G. S. Chirikjian, "The path-of-probability algorithm for steering and feedback control of flexible needles," *Int. Journal of Robotics Research*, vol. 29, no. 7, pp. 813-830, June 2010.
[9] R. Alterovitz, M. Branicky, and K. Goldberg, "Motion planning under uncertainty for image-guided medical needle steering," *Int. Journal of Robotics Research*, vol. 27, no. 11-12, pp. 1361-1374, Nov./Dec. 2008.
[10] R. Alterovitz, S. Patil, and A. Derbakova, "Rapidly-exploring Roadmaps: Weighing exploration vs. refinement in optimal motion planning," in *Proc. IEEE Int. Conf. on Robotics and Automation*, 2011, pp. 3706-3716.
[11] E. Lobaton, J. Zhang, S. Patil, and R. Alterovitz, "Planning curvature-constrained paths to multiple goals using circle sampling," in *Proc. IEEE Int. Conf. on Robotics and Automation*, 2011, pp. 1463-1469.
[12] J. Xu, V. Duindam, and K. Goldberg, "Motion planning for steerable needles in 3D environments with obstacles using rapidly exploring random trees and backchaining," in *Proc. IEEE Int. Conf. on Automation Science and Engineering*, 2008, pp. 41-46.
[13] S. Patil and R. Alterovitz, "Interactive motion planning for steerable needles in 3D environments with obstacles," in *Proc. IEEE RAS/EMBS Int. Conf. Biomedical Robotics and Biomechatronics*, 2010, pp. 893-899.
[14] S. Patil, J. Burgner, R. J. Webster III, and R. Alterovitz, "Needle steering in 3-D via rapid replanning," *IEEE Trans. on Robotics*, in press.
[15] C. Caborni, S. Y. Ko, E. D. Momi, G. Ferrigno, and F. R. Y. Baena, "Risk-based path planning for a steerable flexible probe for neurosurgical intervention," in *Proc. IEEE RAS/EMBS Int. Conf. on Biomedical Robotics and Biomechatronics*, 2012, pp. 866-871.
[16] G. J. Vrooijink, M. Abayazid, S. Patil, R. Alterovitz, and S. Misra, "Needle path planning and steering in a three-dimensional non-static environment using two-dimensional ultrasound images," *Int. Journal of Robotics Research*, in press.
[17] M. C. Bernardes, B. V. Adorno, P. Poignet, and G. A. Borges, "Robot-assisted automatic insertion of steerable needles with closed-loop imaging feedback and intraoperative trajectory replanning," *Mechatronics*, vol. 23, no. 6, pp. 630-645, Sep. 2013.
[18] M. C. Bernardes, B. V. Adorno, G. A. Borges, and P. Poignet, "3D robust online motion planning for steerable needles in dynamic workspaces using duty-cycled rotation," *Journal of Control, Automation and Electrical Systems*, vol. 25, no. 2, pp. 216-227, Apr. 2014.
[19] S. M. LaValle and J. J. Kuffner, "Randomized kinodynamic planning," *Int. Journal of Robotics Research*, vol. 20, no. 5, pp. 378-400, May 2001.
[20] R. J. Webster III, J. S. Kim, N. J. Cowan, G. S. Chirikjian, and A. M. Okamura, "Nonholonomic modeling of needle steering," *Int. Journal of Robotics Research*, vol. 25, no. 5–6, pp. 509–525, May 2006.
[21] K. B. Reed, A. M. Okamura, and N. J. Cowan, "Controlling a robotically steered needle in the presence of torsional friction," in *Proc. IEEE International Conference on Robotics and Automation*, 2009, pp. 3476-3481.
[22] Y. J. Zhao, Y. D. Zhang, and J. P. Shao, "Kinematic modeling and experimental study of flexible needle," *Robot*, vol. 32, no. 5, pp. 666-673, Sep. 2010.

Yan-Jiang Zhao, born in Harbin, China, Nov. 23, 1979, received his B. Sc. degree in Mechanical Engineering from Heilongjiang University of Science and Technology, Harbin, China, in 2003, and his M.Sc. degree in Mechanical and Electrical Engineering, Ph.D. degree in Mechanical Engineering from Harbin University of Science and Technology, Harbin, China, in 2006 and 2012, respectively. Since 2013, he has been a Postdoctoral Research Fellow in the Department of Radiation Oncology, Thomas Jefferson University, Philadelphia, PA, USA. He is currently also an Associated Professor and a Master Tutor in Mechanical and Electrical Engineering of Intelligent Machine Institute, Harbin University of Science and Technology, Harbin, China. His main research interest is medical robotics.

Bardia Konh received his B. S. in 2007 from K. N. Toosi University of Technology and M. Sc. in 2011 from Free University of Science and Research in Tehran, Iran. He is currently a Ph. D. Candidate in the Department of Mechanical Engineering of Temple University in Philadelphia, PA, USA. His research interest is in the design of medical devices using active/smart materials.

Mohammad Honarvar received his B. Sc. and M. Sc. in material science and engineering from Shiraz University, Shiraz, Iran. He is currently a Ph. D. candidate in the Department of Mechanical Engineering of Temple University. His research focus is on the investigation of thermomechanical behavior of Nitinol for actuators in biomedical devices.

Felix Orlando Maria Joseph received his B. E. degree in Instrumentation and Control Engineering from Madras University, M. E. degree in Robotics and HCI from KIST South Korea, Ph. D. in Electrical Engineering from IIT Kanpur, India. Since Feb. 2014, is a Post-Doctoral Research Fellow in the department of Radiation Oncology, University Hospitals, Case Western Reserve University, Cleveland, OH, USA.

Tarun Podder received the B. E. degree from the University of Calcutta, Kolkata, India, in 1988, and M.E. degree from the Indian Institute of Science, Bangalore, India, in 1990, both in Mechanical Engineering, and the Ph. D. degree in Robotics and Automation from the University of Hawaii, Manoa, in 2000. From 2001 to 2006, he was with Rochester Institute of Technology, R. Systems, Inc., Monterey Bay Aquarium Research Institute, and the University of Rochester as a Research Scientist, Research Specialist and Project Manager, Research Fellow, and Research Assistant Professor, respectively. From 2006 to 2012, he was with the Thomas Jefferson University, the University of North Carolina, and East Carolina University as an Assistant Professor, Adjunct Associate Professor and Associate Professor, respectively. Currently, he is an Associate Professor in Department of Radiation Oncology, Case Western Reserve University, Cleveland, OH. His current research interests include dynamics, path planning, and control of robotic and autonomous systems, especially medical robotics and devices. Dr. Podder is a member of the Institute of Electrical and Electronics Engineers, the American Society of Mechanical Engineers, the IEEE Engineering in Medicine and Biology Society, the IEEE Robotics and Automation Society, the American Association of Physicists in Medicine, and the American Society for Therapeutic Radiology and Oncology.

Parsaoran Hutapea received his B. Sc, M. Sc, and Ph. D. in Aerospace Engineering, all from North Carolina State University, Raleigh, North Carolina. He is currently an Associate Professor in the Department of Mechanical Engineering of Temple University in Philadelphia, PA, USA. He is the Directors of Composites Laboratory and the College of Engineering Nano Instrumentation Center.

Adam P. Dicker received his B.A. in Chemistry from Columbia College, New York, NY, in 1984, Ph. D. in Molecular Pharmacology and Therapeutics from Cornell University Graduate School of Medical Sciences, New York, NY, in 1991, and M. D. in Medicine from Cornell University Medical College, New York, NY in 1992. He is the Chair & Professor of Radiation Oncology, Thomas Jefferson University, Philadelphia, PA. He serves as Director, Christine Baxter Research Laboratory for Experimental Cancer Therapies at Jefferson Medical College. He coordinates an interdisciplinary team of oncologists, physicists and scientists focused on multidisciplinary effort to define fundamental mechanisms and targets for combined modality radiation treatment and efficiently translate them to effective innovations in treating cancer patients. He serves as the Chair of the Translational Research Program in the Radiation Therapy Oncology Group (RTOG). He has published numerous papers evaluating signal transduction agents with ionizing radiation and published "first in human" developmental therapeutic trials involving novel signal transduction agents and radiation therapy. Dr. Dicker served as Chair of the Radiation and Cancer Biology Committee of the American Society of Therapeutic Radiation Oncology, and currently is Chairperson of the Radiation Oncology Section of the Clinical Research Subcommittee of AACR. Dr. Dicker serves as the co-Chair-Translational Science Committee for the NCI cooperative group. Dr. Dicker was recently appointed as a member of the Integration Panel for the Prostate Cancer Research Program of the Department of Defense Prostate Cancer Research Program.

Yan Yu received his B. Sc. degree from Queen Mary College and Ph. D. degree from University College, both of University of London, UK, in Physics, in 1983 and 1986, respectively. He also received an MBA degree from University of Rochester, Rochester, NY, USA, in 1998. After completing a clinical fellowship in medical physics, he was on the faculty of the University of Rochester Medical Center from 1994 to 2006. He is currently a Vice Chair, Professor and Director of Medical Physics in the Department of Radiation Oncology, Thomas Jefferson University, Philadelphia, PA, USA. Prof. Yu is a member of the American Association of Physicists in Medicine, the Radiation Research Society, the American Society for Therapeutic Radiology and Oncology, the American Brachytherapy Society, the American Board of Surgery, the American College of Radiology, the Institute of Physics and Engineering in Medicine (Overseas Affiliate member), and Sino-American Network for Therapeutic Radiology and Oncology.